Multi-Tracer Uptake Correction for PET-MR via Aligned-Feature Guidance and Multi-scale Pixel-adaptive Routing

Aocheng Zhong[1†], Haolin Huang[1†], Jing Wang[2,3†], Zhenrong Shen[4], Haiyu Song[1], Junlei Wu[1], Yuhua Zhu[2], Yang Liu[2], Chuantao Zuo[2,3(✉)], and Qian Wang[1,5(✉)]

[1] School of Biomedical Engineering & State Key Laboratory of Advanced Medical Materials and Devices, ShanghaiTech University, Shanghai, China
qianwang@shanghaitech.edu.cn
[2] Department of Nuclear Medicine/PET center, Huashan Hospital, Fudan University, Shanghai, China
[3] Human Phenome Institute, Fudan University, Shanghai, China
zuochuantao@fudan.edu.cn
[4] School of Biomedical Engineering, Shanghai Jiao Tong University, Shanghai, China
[5] Shanghai Clinical Research and Trial Center, Shanghai, China

Abstract. Positron Emission Tomography combined with Magnetic Resonance (PET-MR) imaging has emerged as a promising modality that offers both soft tissue and biochemical function information, while substantially reducing radiation exposure compared to PET-CT imaging. However, systematic clinical evaluations reveal notable discrepancies in standardized uptake value ratios between PET-MR and PET-CT scans, largely due to the inherent limitations of MR-based PET attenuation correction. To address this issue, we propose a unified uptake correction framework to harmonize PET-MR images with PET-CT scans across different tracers. This framework employs a three-stage training scheme. The first stage learns to represent CT features, aiming to capture condensed anatomical patterns associated with PET imaging. The second stage aligns MR features to the fixed CT features learned in the first stage, thereby enabling the transfer of anatomical prior knowledge from CT to MR features. The third stage integrates aligned MR features to guide PET-MR tracer uptake correction and uses a Multi-scale Pixel Routing module to mitigate interference among different tracers. We conduct comprehensive experiments on 70 patients with three distinct tracers to demonstrate the superiority of our framework over existing methods in PET-MR harmonization with PET-CT images. This work represents the first investigation and solution for multi-tracer quantification discrepancies between PET-MR and standard PET-CT, potentially advancing the clinical standardization of PET-MR imaging. Our code will be available at GitHub.

Keywords: PET-MR imaging · Uptake Correction · Multi-Tracer.

† These authors contributed equally to this work.

1 Introduction

The integration of Positron Emission Tomography (PET) with Magnetic Resonance (PET-MR) represents a revolutionary advancement in clinical molecular imaging, attracting significant research attention and expanding clinical applications [1, 2]. These hybrid systems offer distinct advantages such as superior soft tissue contrast from MRI, reduced ionizing radiation exposure, and the capacity for simultaneous multiparametric metabolic and anatomical assessments [3, 4]. In clinical practice, radiologists often presume quantitative equivalence between PET-MR and PET combined with Computed Tomography (PET-CT). Consequently, they routinely interpret PET-MR images using quantification criteria established for PET-CT, the latter being a cornerstone of molecular imaging due to its high sensitivity and robust quantitative evaluation of physiological and pathological processes, particularly in neurology [5–8].

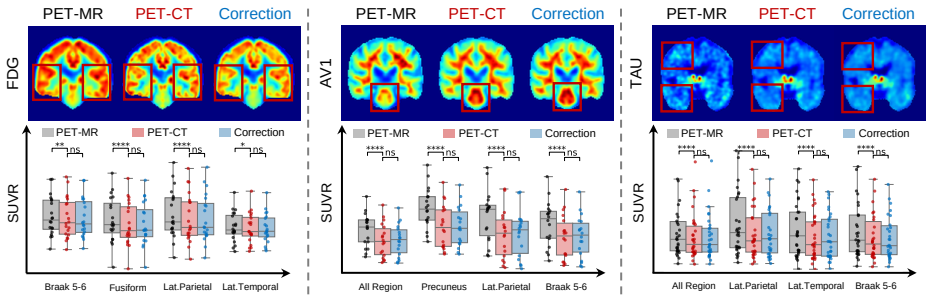

Fig. 1. Visual and statistically significant differences in standardized uptake value ratio (SUVR) between PET-MR and PET-CT imaging across different tracers. The proposed framework can correct PET-MR toward PET-CT to mitigate these differences.

However, systematic clinical evaluations demonstrate significant discrepancies in standardized uptake value ratios (SUVRs) between PET-MR and PET-CT across diverse tracers, as illustrated in Fig. 1. This quantitative inconsistency may originate from vendor-specific MR-based attenuation correction (AC) methods. In PET-CT systems, the inherent correlation between X-ray attenuation coefficients in CT and tissue electron density ensures precise AC for reliable PET reconstruction [9]. In contrast, MR signal intensity lacks direct associations with electron density or atomic composition, forcing AC algorithms to estimate attenuation properties through segmentation or atlas-based templates. Such approximations introduce systematic errors in PET quantification [2]. These discrepancies, often overlooked in clinical practice, pose significant risks of diagnostic inaccuracies when applying PET-CT-derived quantification criteria directly to PET-MR images. Therefore, there is an urgent need to develop methods that can correct PET-MR images toward PET-CT across different tracers.

Image restoration (IR) using deep learning can transform low-quality medical images into high-quality ones [10], serving as a feasible solution to address the issue above. In the context of PET imaging, several studies have demonstrated success in applying IR techniques for low-dose PET reconstruction, where standard-dose images are restored from low-dose images [11,12]. However, these approaches primarily focus on PET data alone, often overlooking the valuable anatomical prior information from accompanying structural images. Furthermore, many PET restoration methods are designed for a specific tracer, leading to significant performance degradation when applied to other tracers due to their uptake distribution differences caused by distinct biochemical properties. Given that different tracers are often scanned on the same PET system in clinical settings, it is inefficient to deploy and maintain separate models for each tracer. Thus, developing algorithms capable of handling multiple tracers simultaneously is essential for clinical practice.

To address these challenges, we propose the first PET-MR tracer uptake correction framework to harmonize PET-MR with PET-CT images across different tracers with a unified model by leveraging anatomical information from structural images. Our primary contributions are summarized as follows: (1) We develop a novel PET-MR tracer uptake correction framework, which addresses multi-tracer quantification discrepancies between PET-MR and standard PET-CT. (2) We improve PET-MR tracer uptake correction by leveraging aligned MR features that incorporate imaging-related prior knowledge transferred from CT to MR, thereby mitigating the inherent limitations of MR in PET imaging. (3) We propose a Multi-scale Pixel Routing module to reduce interference between different tracers by assigning conflicting tasks to distinct multi-scale network paths. (4) Experiments demonstrate that our framework outperforms other IR methods in PET-MR tracer uptake correction across multiple tracers, making it a valuable tool for standardizing the quantification of PET-MR and PET-CT.

2 Method

As illustrated in Fig. 2, our method employs a three-stage training scheme to address the quantification discrepancies between PET-MR and standard PET-CT. Firstly, the framework performs CT feature representation learning to extract essential anatomical information for PET reconstruction. Secondly, by using the learned CT representations as reference patterns, the framework aligns MR features to CT features, enabling the transfer of anatomical prior knowledge from CT to MR features. The final stage incorporates the aligned MR features into a U-Net architecture [13] to perform PET-MR tracer uptake correction, and leverages an MsPR module to mitigate interference between different tracers. Through this systematic multi-stage training scheme, our proposed method effectively bridges the quantification gap between PET-MR and PET-CT across multiple tracer applications.

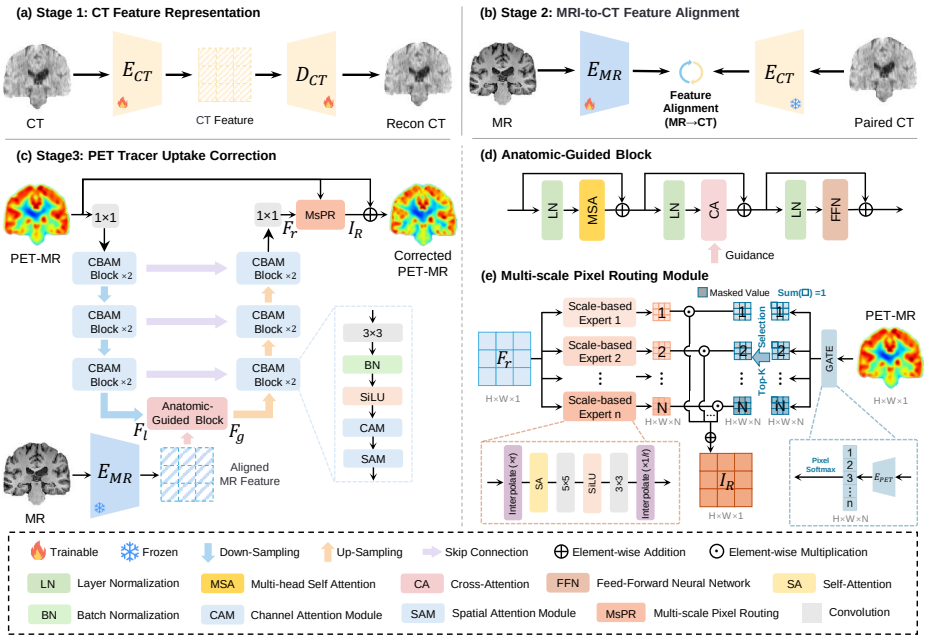

Fig. 2. The proposed framework adopts a three-stage training scheme: (a) CT feature representation to extract essential anatomical information, (b) MR-to-CT feature alignment, and (c) PET-MR tracer uptake correction with aligned MR features.

2.1 CT Feature Representation

The first stage of our method focuses on learning the CT feature representations directly associated with PET imaging, which serve as anatomical prior knowledge for the next stage. As shown in Fig. 2(a), we utilize an Autoencoder (AE) [14] with a Visual Transformer (ViT) architecture [15] to capture long-range dependencies and contextual features [16] for CT image representation. The AE first partitions each CT image into $M = 1024$ non-overlapping patches and then converts them into an $M \times D$ latent representation by the encoder E_{CT}, where $D = 512$ represents the embedding dimension. To obtain CT features, the AE reconstructs CT images from their latent representations by the decoder D_{CT}, and employs a pixel-wise ℓ_2 loss between the input and reconstructed CT images. This design can capture a reliable representation of CT, thereby establishing a robust foundation for anatomical knowledge transfer in the subsequent stage.

2.2 MR-to-CT Feature Alignment

Unlike CT images, MR images lack the tissue density information critical to PET AC, thus introducing inevitable inaccuracies in PET reconstruction [17]. To address this limitation, we propose a feature alignment strategy that transfers

anatomical knowledge from CT to MR, establishing a consistent structural basis for subsequent PET-MR tracer uptake correction. As shown in Fig. 2(b), we firstly use the pre-trained CT encoder E_{CT} from the first stage to generate anatomical reference patterns F_{CT}. Then we train an MRI encoder E_{MR} with the same architecture to convert MR images into MR features F_{MR} that are aligned with CT feature representations F_{CT}.

To achieve precise feature alignment, we employ a contrastive learning framework instead of conventional distribution matching metrics like Kullback-Leibler (KL) divergence [18]. Specifically, our approach enables patch-level feature alignment using two complementary loss terms. The positive pair loss encourages feature correspondence between the patches from the same location in the MR and CT images:

$$\mathcal{L}_{\mathrm{pos}} = \frac{1}{M} \sum_{j=1}^{M} \left(\left\| F_{\mathrm{CT}}^{j} - F_{\mathrm{MR}}^{j} \right\|_2^2 \right), \tag{1}$$

where F_{MR}^{j} and F_{CT}^{j} denote MR and CT features from the j-th patch of the same subject, respectively. Conversely, the negative pair loss prevents spurious alignment between non-corresponding patches:

$$\mathcal{L}_{\mathrm{neg}} = \frac{1}{M \cdot M} \sum_{j=1}^{M} \sum_{k=1}^{M} \left(\max(0, \mathrm{margin} - \left\| F_{\mathrm{CT}}^{j} - F_{\mathrm{MR}}^{k} \right\|_2^2) \right) \quad [j \neq k], \tag{2}$$

where we empirically set margin to 1.0. The final contrastive loss combines both loss terms with equal weights.

2.3 PET-MR Tracer Uptake Correction

The network architecture of our PET Tracer Uptake correction model is illustrated in Fig. 2(c). It transforms the input PET-MR image into a corrected one through several key processing stages. Initially, a shallow feature map is extracted from the input image via a 1×1 convolution layer and is then processed by three consecutive CBAM blocks [19] to produce a latent representation F_l. To incorporate anatomic guidance, we leverage the aligned MR features F_{MR} as the guidance to inject PET-CT characteristics into the PET-MR latent space via a anatomic-guided block as shown in Fig. 2(d), resulting in a refined features F_g. Subsequently, a decoder reconstructs a high-resolution feature map F_d from F_g via three symmetrical CBAM blocks as well as skip connections to preserve fine-grained details from the encoder, followed by a 1×1 convolution to transform F_d into a residual feature map F_r. The network has a refinement module to address inter-tracer interference by the proposed Multi-scale Pixel Routing module, which operates on F_r to generate a residual image with the input image size. The final corrected image is obtained by combining this residual image with the input image. This stage is optimized using a composite loss function that combines a pixel-wise ℓ_2 loss with a perceptual similarity loss L_{lpips}.

Multi-scale Pixel Routing As shown in Fig. 2(e), the proposed Multi-scale Pixel Routing (MsPR) module is designed in a Mixture of Experts [20] fashion in order to mitigate inter-tracer interference in the shared network parameters. Considering the fine-grained nature of tracer uptake correction, MsPR module assigns each pixel from the input PET-MR image to the most suitable expert networks based on the routing instructions. Specifically, MsPR module implements $N = 7$ parallel multi-scale expert networks to process the residual feature map F_r. The processing pipeline of each expert network starts with a spatial upsampling with a random factor r and ends with a spatial downsampling with factor $\frac{1}{r}$. The sampling rates for parallel expert networks are configured as follows: $r = \left\{\frac{1}{4}, \frac{1}{3}, \frac{1}{2}, 1, 2, 3, 4\right\}$. MsPR module generates routing instructions ϕ from the $H \times W \times 1$ input PET-MR image by encoding it into a $H \times W \times N$ feature map and applying softmax activation along the channel dimension. A top-K ($K = 4$) selection mechanism is then employed to each feature vector at different spatial locations in ϕ, masking $N - K$ values along the channel dimension at each spatial location. After the top-K selection, the feature maps of different channels are used as gating maps for different expert networks. This adaptive routing strategy allows the network to dynamically combine effective features from different spatial locations to produce the optimal residual image I_R for different tracers, thereby enhancing uptake correction precision.

3 Experiments and Results

3.1 Dataset and Experimental Setup

Dataset. We prospectively collect imaging data from 70 patients at an anonymous hospital, encompassing one commonly used tracer in clinical practice, along with two specific tracers frequently utilized in neuroimaging research: ^{18}F-FDG (FDG; n=20), ^{18}F-AV1 (AV1; n=20), and ^{18}F-PM-PBB3 (TAU; n=30). Each patient underwent PET/CT and then immediately PET/MR scans in a single visit to hospital. All acquired images are spatially normalized to the Montreal Neurological Institute (MNI) 152 template and skull-stripped to isolate brain tissue. The preprocessed 3D volumes are subsequently divided into 2D slices and cropped to 128×128 pixels. This preprocessing pipeline produces matched quartets of PET-MR and PET-CT images for each subject, establishing a comprehensive dataset for training and evaluation.

Implementation Details. To ensure a comprehensive evaluation, all experiments are conducted using a five-fold cross-validation at the subject level (4 FDG, 4 AV1, and 6 TAU patients per fold) on an NVIDIA A100 GPU using PyTorch [21]. For optimization, we employ the Adam optimizer [22] with Cosine Annealing learning rate scheduling [23] across all three stages. Training consisted of [200, 100, 100] epochs with initial learning rates of [1×10^{-4}, 1×10^{-3}, 1×10^{-4}] decaying to [1×10^{-6}, 1×10^{-4}, 1×10^{-5}] using cosine annealing from epochs [20, 10, 10], and batch sizes of [8, 8, 32] for Stages 1-3 respectively.

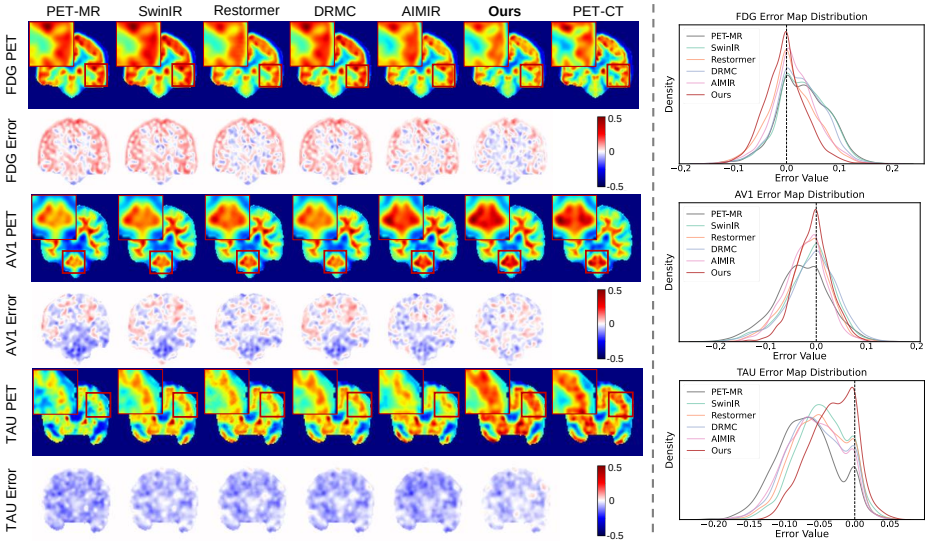

Fig. 3. Qualitative comparison of our framework with other IR methods across three tracers. The density plots display the distribution of pixel errors between corrected images and PET-CT images, where curves closer to zero indicate superior correction.

Table 1. Quantitative comparison between our framework and other IR methods across three tracers (FDG, AV1, and TAU). The results are in the "mean ± standard deviation" format with the best results marked in bold.

Model	FDG		AV1		TAU	
	PSNR	SSIM%	PSNR	SSIM%	PSNR	SSIM%
PET-MR	$36.18_{\pm 0.64}$	$98.59_{\pm 0.14}$	$31.41_{\pm 0.70}$	$97.39_{\pm 0.31}$	$34.54_{\pm 2.09}$	$96.18_{\pm 0.70}$
SwinIR [24]	$35.81_{\pm 0.87}$	$98.51_{\pm 0.16}$	$33.27_{\pm 0.54}$	$97.99_{\pm 0.23}$	$36.02_{\pm 1.87}$	$97.26_{\pm 0.51}$
Restormer [25]	$36.27_{\pm 0.57}$	$98.38_{\pm 0.12}$	$33.82_{\pm 0.99}$	$97.76_{\pm 0.17}$	$36.25_{\pm 1.67}$	$97.18_{\pm 0.42}$
DRMC [26]	$36.40_{\pm 0.85}$	$98.66_{\pm 0.19}$	$33.42_{\pm 0.89}$	$97.98_{\pm 0.24}$	$36.45_{\pm 1.82}$	$97.31_{\pm 0.44}$
AIMIR [11]	$36.53_{\pm 0.75}$	$98.48_{\pm 0.15}$	$34.07_{\pm 0.92}$	$98.09_{\pm 0.16}$	$36.36_{\pm 1.68}$	$97.45_{\pm 0.41}$
Ours	$\mathbf{37.39_{\pm 0.63}}$	$\mathbf{98.82_{\pm 0.13}}$	$\mathbf{35.00_{\pm 1.23}}$	$\mathbf{98.39_{\pm 0.18}}$	$\mathbf{36.98_{\pm 1.59}}$	$\mathbf{97.69_{\pm 0.37}}$

3.2 Comparison with SOTA Methods

To evaluate our proposed framework, we compare it with state-of-the-art (SOTA) IR methods, including SwinIR [24], Restormer [25], DRMC [26], and AIMIR [11]. SwinIR and Restormer demonstrate robust performance in natural image restoration, DRMC specializes in multi-center PET restoration, and AIMIR is tailored for multi-modal medical image restoration. All methods are implemented as universal models to handle multiple tracers simultaneously.

Qualitative comparison results across different tracers are illustrated in Fig. 3. For FDG and AV1, notable uptake differences in PET-MR compared to PET-CT are observed separately in the gray matter (higher uptake) and brainstem (lower uptake) regions. While SwinIR and DRMC show negligible correction

effects, Restormer and AIMIR achieve only partial correction. In contrast, our method successfully restores appropriate uptake patterns for both tracers. For TAU, which exhibits globally lower uptake patterns, all methods achieve certain level of corrections but our method consistently yields the most substantial improvements. Quantitative results in Table 1 further corroborate the superior performance of our method, as evidenced by consistently higher PSNR and SSIM metrics across all tracers. Notably, comparative methods often exhibit tracer-specific performance variations. For example, DRMC outperforms Restormer on FDG but underperforms on AV1. These results indicate the capability of our method in effectively mitigating inter-tracer interference, thereby enabling consistent performance across different tracers.

Table 2. Ablation study of the key components of the proposed framework, including (a) Structural Guidance (SG), (b) MR-to-CT Feature Alignment (M2C), (c) Multi-scale Pixel Routing (MsPR).

Configuration			FDG		AV1		TAU	
SG	M2C	MsPR	PSNR (dB)	SSIM%	PSNR (dB)	SSIM%	PSNR (dB)	SSIM%
×	×	×	$36.92_{\pm 0.67}$	$98.68_{\pm 0.18}$	$34.52_{\pm 1.12}$	$98.27_{\pm 0.16}$	$36.53_{\pm 1.53}$	$97.57_{\pm 0.39}$
✓	×	×	$37.11_{\pm 0.65}$	$98.76_{\pm 0.12}$	$34.67_{\pm 1.19}$	$98.32_{\pm 0.22}$	$36.65_{\pm 1.57}$	$97.62_{\pm 0.37}$
✓	✓	×	$37.25_{\pm 0.67}$	$98.79_{\pm 0.14}$	$34.80_{\pm 1.20}$	$98.36_{\pm 0.18}$	$36.76_{\pm 1.58}$	$97.65_{\pm 0.37}$
✓	✓	✓	$\mathbf{37.39_{\pm 0.63}}$	$\mathbf{98.82_{\pm 0.13}}$	$\mathbf{35.00_{\pm 1.23}}$	$\mathbf{98.39_{\pm 0.18}}$	$\mathbf{36.98_{\pm 1.59}}$	$\mathbf{97.69_{\pm 0.37}}$

3.3 Ablation Study

We conduct a comprehensive ablation study to evaluate the effectiveness of our proposed three-stage training strategy. As illustrated in Table 2, starting with CBAM-block-based U-Net as the baseline, we sequentially integrate each key component to quantitatively assess their contributions. The initial integration of structural guidance from MR images without feature alignment can yield a 0.15 dB improvement in average PSNR and a 0.06% increase in average SSIM across all three tracers, highlighting the enhancement of corrected image quality via structural guidance. Subsequently, implementing MR-to-CT feature alignment further boosts the model performance by increasing the average PSNR from 36.14 dB to 36.27 dB, demonstrating the effectiveness of the feature alignment strategy in transferring useful prior information from CT to MR. Finally, the incorporation of MsPR module brings in substantial performance gains with an average PSNR of 36.46 dB and an average SSIM of 98.30%, showcasing the efficacy of our proposed MsPR module in reducing inter-tracer interference.

4 Conclusion and Discussion

In this work, we present the first unified framework to address the quantification discrepancies between PET-MR and PET-CT imaging across multiple tracers.

It adopts a three-stage training scheme, and leverages the aligned MR features guidance and a novel Multi-scale Pixel Routing module to effectively harmonize PET-MR quantification with PET-CT standards regardless of inter-tracer interference. Experiments demonstrate that our method consistently outperforms existing SOTA methods in both quantitative metrics and visual quality. Future work will focus on validating the model's robustness across a broader range of tracers in larger scales to further establish its clinical applicability.

Acknowledgments. This work was partially supported by National Natural Science Foundation of China (82394432, 82272039, 82021002, 82394434), STI2030-Major Projects (2022ZD0211606) and AI4S Initiative and HPC Platform of ShanghaiTech University.

Disclosure of Interests. The authors have no competing interests to declare that are relevant to the content of this article.

References

1. Zaharchuk, G.: Next generation research applications for hybrid pet/mr and pet/ct imaging using deep learning. European journal of nuclear medicine and molecular imaging **46**(13), 2700–2707 (2019)
2. Krokos, G., MacKewn, J., Dunn, J., Marsden, P.: A review of pet attenuation correction methods for pet-mr. EJNMMI physics **10**(1), 52 (2023)
3. Ehman, E.C., Johnson, G.B., Villanueva-Meyer, J.E., Cha, S., Leynes, A.P., Larson, P.E.Z., Hope, T.A.: Pet/mri: where might it replace pet/ct? Journal of Magnetic Resonance Imaging **46**(5), 1247–1262 (2017)
4. Zhu, T., Das, S., Wong, T.Z.: Integration of pet/mr hybrid imaging into radiation therapy treatment. Magnetic Resonance Imaging Clinics **25**(2), 377–430 (2017)
5. Golan, H., Volkov, O., Shalom, E.: Nuclear imaging in parkinson's disease: The past, the present, and the future. Journal of the Neurological Sciences **436**, 120220 (2022)
6. Huang, H., Shen, Z., Wang, J., Wang, X., Lu, J., Lin, H., Ge, J., Zuo, C., Wang, Q.: Metaad: Metabolism-aware anomaly detection for parkinson's disease in 3d 18 f-fdg pet. In: International Conference on Medical Image Computing and Computer-Assisted Intervention. pp. 291–301. Springer (2024)
7. Shen, Z., Wang, J., Huang, H., Lu, J., Ge, J., Xiong, H., Wu, P., Ju, Z., Lin, H., Zhu, Y., et al.: Cross-modality pet image synthesis for parkinson's disease diagnosis: a leap from [18f] fdg to [11c] cft. European Journal of Nuclear Medicine and Molecular Imaging pp. 1–10 (2025)
8. Tai, Y.F., Piccini, P.: Applications of positron emission tomography (pet) in neurology. Journal of Neurology, Neurosurgery & Psychiatry **75**(5), 669–676 (2004)
9. Carney, J.P., Townsend, D.W., Rappoport, V., Bendriem, B.: Method for transforming ct images for attenuation correction in pet/ct imaging. Medical physics **33**(4), 976–983 (2006)
10. Jiang, J., Zuo, Z., Wu, G., Jiang, K., Liu, X.: A survey on all-in-one image restoration: Taxonomy, evaluation and future trends. arXiv preprint arXiv:2410.15067 (2024)

11. Yang, Z., Chen, H., Qian, Z., Yi, Y., Zhang, H., Zhao, D., Wei, B., Xu, Y.: All-in-one medical image restoration via task-adaptive routing. In: International Conference on Medical Image Computing and Computer-Assisted Intervention. pp. 67–77. Springer (2024)
12. Xie, H., Gan, W., Zhou, B., Chen, M.K., Kulon, M., Boustani, A., Spencer, B.A., Bayerlein, R., Ji, W., Chen, X., et al.: Dose-aware diffusion model for 3d low-dose pet: multi-institutional validation with reader study and real low-dose data. arXiv preprint arXiv:2405.12996 (2024)
13. Ronneberger, O., Fischer, P., Brox, T.: U-net: Convolutional networks for biomedical image segmentation. In: Medical Image Computing and Computer-Assisted Intervention–MICCAI 2015: 18th International Conference, Munich, Germany, October 5-9, 2015, Proceedings, Part III 18. pp. 234–241. Springer (2015)
14. Rumelhart, D.E., Hinton, G.E., Williams, R.J.: Learning internal representations by error propagation, p. 318–362. MIT Press, Cambridge, MA, USA (1986)
15. Dosovitskiy, A., Beyer, L., Kolesnikov, A., Weissenborn, D., Zhai, X., Unterthiner, T., Dehghani, M., Minderer, M., Heigold, G., Gelly, S., et al.: An image is worth 16x16 words: Transformers for image recognition at scale. In: International Conference on Learning Representations (2021)
16. Chen, T., Li, B., Zeng, J.: Learning traces by yourself: Blind image forgery localization via anomaly detection with vit-vae. IEEE Signal Processing Letters **30**, 150–154 (2023)
17. Zheng, J., Shen, Z., Zhang, L., Chen, Q.: Structure-guided mr-to-ct synthesis with spatial and semantic alignments for attenuation correction of whole-body pet/mr imaging. arXiv preprint arXiv:2411.17488 (2024)
18. Kullback, S.: Kullback-leibler divergence (1951)
19. Woo, S., Park, J., Lee, J.Y., Kweon, I.S.: Cbam: Convolutional block attention module. In: Proceedings of the European conference on computer vision (ECCV). pp. 3–19 (2018)
20. Jacobs, R.A., Jordan, M.I., Nowlan, S.J., Hinton, G.E.: Adaptive mixtures of local experts. Neural computation **3**(1), 79–87 (1991)
21. Paszke, A., Gross, S., Massa, F., Lerer, A., Bradbury, J., Chanan, G., Killeen, T., Lin, Z., Gimelshein, N., Antiga, L., et al.: Pytorch: An imperative style, high-performance deep learning library. Advances in neural information processing systems **32** (2019)
22. Kingma, D.P.: Adam: A method for stochastic optimization. arXiv preprint arXiv:1412.6980 (2014)
23. Loshchilov, I., Hutter, F.: Sgdr: Stochastic gradient descent with warm restarts. arXiv preprint arXiv:1608.03983 (2016)
24. Liang, J., Cao, J., Sun, G., Zhang, K., Van Gool, L., Timofte, R.: Swinir: Image restoration using swin transformer. In: Proceedings of the IEEE/CVF international conference on computer vision. pp. 1833–1844 (2021)
25. Zamir, S.W., Arora, A., Khan, S., Hayat, M., Khan, F.S., Yang, M.H.: Restormer: Efficient transformer for high-resolution image restoration. In: Proceedings of the IEEE/CVF conference on computer vision and pattern recognition. pp. 5728–5739 (2022)
26. Yang, Z., Zhou, Y., Zhang, H., Wei, B., Fan, Y., Xu, Y.: Drmc: A generalist model with dynamic routing for multi-center pet image synthesis. In: International Conference on Medical Image Computing and Computer-Assisted Intervention. pp. 36–46. Springer (2023)